Industrial Electrical Engineering and Automation

PMSM diagnostics and prognostics

Evaluation of an on-line method based on high frequency current response

Julius Björngreen

Division of Industrial Electrical Engineering and Automation
Faculty of Engineering, Lund University

Master Thesis

PMSM diagnostics and prognostics

Evaluation of an on-line method based on
high frequency current response

Julius Björngreen

Supervisor (Volvo AB)   Zhe Huang
Supervisor (LTH)   Avo Reinap

Examiner (LTH)   Mats Alaküla

LUNDS UNIVERSITET
Lunds Tekniska Högskola

Abstract

This thesis covers and evaluates a stator insulation fault detection method for Permanent Magnetised Synchronous Machines (PMSMs). The method could be implemented on-line and is based on using the power converter in an electric or hybrid vehicle to measure the State of Health (SoH) of the stator insulation of the PMSM. This is done through measurements of the high frequency current response that occurs when the PMSM is subjected to a voltage pulse from the power converter. The high frequency content of this current response is related to the parasitic capacitances of the PMSM and thereby also reflect the quality of the stator insulation. It is shown, in this thesis, that small impedance changes, corresponding to degradation and an early developing fault, can be detected with high repeatability and accuracy.

Acknowledgements

My first thanks goes to Zhe Huang, my supervisor from Volvo, who came up with the idea for this thesis and provided great discussions and regular contact during the whole thesis project. Secondly I thank my supervisor from LTH, Associate Professor Avo Reinap, who always found the time to discuss issues and provide advice. I also thank my examiner Professor Mats Alaküla for all valuable input and advice. A large thank you goes to Sebastian Hall who above all helped me a lot with the LabView programming of the CompactRIO system for the motor control. Sebastian also deserve a great thanks for all his tips and all productive discussions with bouncing of ideas and so on. A big thanks also goes to Getachew Darge, the committed enthusiast, who provides, keeps track of and maintains all instruments, equipment and tools. He was of great help especially, but far from only, when the test rig with the electric machine was set up when cables, specific tools and advice on good practical solutions were needed.

List of Abbreviations

AC Alternating Current

AD Analogue to Digital

ADC Analogue to Digital Converter

cRIO Compact Reconfigurable Input Output

CSA Current Signature Analysis

DC Direct Current

EV Electric Vehicle

FEM Finite Element Method

FFT Fast Fourier Transform

FPGA Field-Programmable Gate Array

IEEE Institute of Electrical and Electronics Engineers

IGBT Insulated-Gate Bipolar Transistor

IM Induction Motor

LTH Faculty of Engineering - Lund University

MS\s Mega Samples per second

n\a not available

PD-test Partial Discharge Test

PMSM Permanent Magnetised Synchronous Machine

PWM Pulse Width Modulated

RAM Random Access Memory

rpm revolutions per minute

SoH State of Health

VSC Voltage Source Converter

List of Figures

List of Tables

Contents

Chapter 1

Introduction

1.1 Background

Electrical machines are generally highly reliable. However, the electrical machine that acts as motor or generator in Electric Vehicles (EVs) is used at different, much more varied, load conditions compared to a traditional electrical machine in a factory. The operation of the EV is often such that the electrical machine in it is used at quickly altered load conditions and is subjected to multiple stresses such as thermal, mechanical and ambient stresses. The fast switching of modern power electronics such as Insulated-Gate Bipolar Transistors (IGBTs) in the power converter also puts further stress on the electrical machine. The electrical machine in EVs is also required to provide as high power density as possible in order to get a high return on investment. Since the weight and size of the electric machine is designed to be as small as possible, while still maintaining its function, the electrical machine is often used near its rated values. This includes both the rated values for continuous as well as peak torque and power. At the same time the EV is required to deliver high up-time and an unscheduled stop of a machine is unacceptable and is associated with large economic losses and safety issues.

With this in mind a reliable method for monitoring the SoH of electrical machines would be of great interest in this aspect. If a fault can be detected before it occurs it would certainly be beneficial compared to detecting it by noticing the machine not working. It would also be beneficial if this monitoring could be done on line without needing to take the vehicle to a workshop or disconnect the electrical machine.

A critical aspect of electric traction motor drives is the stator insulation system. According to different studies stator winding insulation failures account for about a third of all electric motor failures. In particular the most comprehensive study done on the subject, that surveyed 7500 large Induction Motors (IMs), found that 37 % of all failures were related to stator winding problems[10][p131]. For this reason, monitoring of the stator insulation is deemed highly interesting.

The stator insulation is subjected to mechanical, thermal, ambient and electrical stresses and the lifetime of the stator depends heavily on how much it is subjected to these stresses. The degradation of the stator insulation is often a slow process. However, as the stator insulation deteriorates, the parasitic insulation capacitances change [7][9]. An ability to monitor the parasitic capacitances, namely the phase-to-phase, phase-to-core and turn-to-turn capacitances of the electrical machine, would consequentially result in an ability to be able to detect degradation of the stator insulation. The method proposed in this thesis relies on measuring these capacitances indirectly from measuring the high frequency current response that appears when a voltage step is applied over the motor windings.

1.2   Disposition

Below follows a list that gives a short introduction to the content of all chapters in this thesis.

- Chapter 1, Introduction, gives a background and motivation to the proposed fault detection technique and presents previous work.

- Chapter 2, Method description and theory, explains the proposed fault detection method and the relevant theory behind it.

- Chapter 3, Electrical model, presents a simulation model that has been developed in order to simulate the proposed method in Lt-SPICE.

- Chapter 4, Experimental procedure , presents how the tests and experiments were carried out, the experimental set-up and equipment that was used.

- Chapter 5, Analysis and results, goes through the results, the post processing of data, the accuracy of the measurements and addresses how to interpret the data.

- Chapter 6, Comparison of model and measurements, compares the experimental results obtained with the simulated results gathered from the electrical model.

- Chapter 7, Conclusion and future work, concludes the thesis and suggests future work.

1.3   Working methodology

The working methodology used during this master thesis project is divided into phases. These phases are listed and shortly described below:

- After a goal document and a project plan were approved this master thesis project started with a literature study. The literature studied consists of presented articles that address fault detection techniques and diagnostics methods for electrical machines. The literature study also includes reading

up on relevant theory.

- Phase two of this master thesis project consists of making measurements on the PMSM tested during this project with lab equipment such as impedance analyser, oscilloscope etcetera. The purpose of these measurements were to be a basis for the construction of an equivalent circuit model of the test object in LtSPICE. These measurements also provided basis for the choosing of what components to use for the construction of the measuring equipment. This phase also include programming of the motor control software in Labview.

- The third phase consists of building and programming the equipment used for making measurements. The programming of the Red Pitaya that is used for making and storing the measurements are written in MATLAB.

- The fourth phase includes the actual measuring and the analysis of the measured data. Lots of different measurements under different conditions are made and the data analysis is done in MATLAB. After the data analysis a comparison between the obtained measurement results and the LtSPICE simulation model is done. This is followed by evaluation and improvement of the simulation model.

- The fifth and last phase consists of writing the final report. This was to some extent done in parallel with earlier phases, especially the data analysis phase, but most of the report writing is done last when all data was gathered and analysed.

1.4 Previous Work

1.4.1 Today existing diagnostic methods

On the market today there are some methods for determining the SoH of an electrical machine. However the methods that are used today are often either expensive or require disconnection of the motor and thus has to be done in a workshop. Methods like these that require out-take and/or has to be done in a workshop are called off-line methods. According to [14] most of the industrially accepted test are off-line fault detection methods and include the off-line surge test, the Direct Current (DC)-conductivity test, the insulation resistance test,polarisation index and the DC/AC HIPot test [14]. Those methods are as stated off-line methods and if possible an on-line method would certainly be preferable to an off-line method since less or no intervention is needed in an on-line method. An industrially accepted on-line test is the Partial Discharge Test (PD-test). This test

unfortunately also has disadvantages. One of them is that the method requires expensive measurement equipment.

1.4.2   On-line diagnostic methods

There are some on-line fault detection techniques that have been presented but not considered industrially accepted. A selection of these are: a method for detecting turn faults through Current Signature Analysis (CSA) investigated in [5], an on-line version of the Surge Test investigated in [4] and a method which involves measuring and evaluating the leakage current between connector and ground to determine phase-to-ground insulation, presented in [13]. These methods are not discussed further in this thesis but are all available on the web at Institute of Electrical and Electronics Engineers (IEEE)-explorer which is IEEEs database for published articles and writings.

Different authors have published articles where the test methods are quite similar to the one proposed in this thesis. All of the methods presented however, that I, the author of this thesis have found, are made on IMs. In this thesis the proposed method is instead applied on a PMSM. In [14] experiments somewhat similar to the ones made in this thesis on a PMSM are done on a 5.5 kW, 2-pole, squirrel-cage induction machine.

1.5   Purpose

The purpose of this master thesis project is to evaluate the proposed fault detection method and determine if the method can be implemented on a PMSM. The work includes making experimental tests and modelling in a simulation program (LtSPICE). The work will also include an investigation on what the minimum hardware requirements would be for implementing the method in a vehicle. The equipment in a vehicle today is most likely too slow to be able to make the measurements required. However the development of this equipment goes forward and the costs get lower. In the future there could be a high possibility that this method is deemed economically viable.

1.6   Delimitations

This thesis project is about evaluating the specific fault detection method that is investigated in this thesis. It does not include comparing this method with other fault detection methods. This thesis does neither include any FEM analysis or advanced modelling of the detailed impedance structure at turn-to-turn level of the stator insulation.

Chapter 2

Method description and theory

2.1 Theory

There is no limit to how long this chapter could be made if everything related to fault detection techniques and electric machine construction regarding stator insulation were to be addressed. For this I refer to any book on the subject for instance "Electrical insulation for rotating Machines - Design, Evaluation, Testing and Repair"[10].Great effort has been taken to keep this chapter rather short but still, in a short way, give an answer to what actually is measured and how that is related to the SoH of the electrical machine. This chapter shortly addresses the definition of parasitic capacitances in a PMSM , the stator insulation of a PMSM as well as the equations used in this thesis project.

2.1.1 Inverter fed electrical machines

As stated in the introduction, electrical machines are generally highly reliable. However an electrical three phase machine in a vehicle is subjected to more electrical stress of a transient nature compared to a machine that is connected to the conventional sinusoidal voltage from the power grid. A three phase electrical machine in a vehicle is instead controlled with a switched power supply. This switched power supply is often Pulse Width Modulated (PWM) with a Voltage Source Converter (VSC). When the electrical machine in the vehicle acts as a motor the VSC is used as an inverter to convert DC from the battery into Alternating Current (AC) which is then converted by the electrical machine into mechanical energy used for traction of the vehicle. However, an inverter does not produce an ideal sinusoidal voltage but rather one with high voltage derivatives, common mode voltages and currents as a result of its operating principals [8]. These high

current derivatives, common mode voltages and currents puts further electrical stress on the electrical machine and produce unwanted harmonics.

2.1.2   Stator of an electrical machine

In a PMSM and in most electrical machines which can act as a motor and a generator the stator includes three main components. These are the copper conductors, the stator core and the stator insulation.

When a PMSM rotates, the rotating magnetic field created by the rotor induces a voltage in the copper conductors. When acting as a motor or a generator, a controlled external voltage is sent through the copper conductors creating a torque that together with an external torque on the machine axle makes the rotor rotate. The dimensions of the copper conductors are highly related to the performance of the electric machine and the copper conductors need to be able to carry all current required without overheating. The stator core concentrates the magnetic field created by the rotor.

The copper conductors and the stator core are thus active components in the sense that they make the electric machine function and sizing of these two components is highly related to the maximum power output of the machine. The stator insulation is instead passive. It does not produce a magnetic field nor does it guide a path of one. Its purpose is instead to prevent short circuits and separate conductors from other conductors or from the stator core. Increasing the size of the insulation does not help in producing torque or current but increases the machine size and cost and lowers the efficiency of the machine. The insulation is still very much needed but from a design point of view one would want it to be as small as possible [10, p131].

2.1.3   Stator insulation

The stator winding insulation system has as previously mentioned the task of preventing short circuits from occurring. The insulation system also has other purposes one being to keep the copper conductors from vibrating due to the magnetic forces that are applied. In electrical machines that are not actively cooled in another way the stator insulation also has the task to transport heat from the conductors. This means that the stator insulation should have low electric conductivity but high thermal conductivity. The stator insulation is primarily made up of three components. Groundwall insulation which is insulation between the stator core and the windings, turn insulation, which is insulation between turns and strand insulation, which is insulation between different strands. Additional to these forms of insulation some machines also have an insulation form called slot divider [10, p12].

Strand insulation

The strand insulations purpose in mainly to reduce skin effect which is a tendency for current not to flow through the centre of the conductor and not using the whole surface area of it. To reduce this effect a common way is to split a large conductor into many thin ones. This effect is only in play for large conductors and thus large machines. By replacing larger conductors with more smaller ones like this, Eddy currents are also reduced which also is a source for loses [10, p13-14].

Turn insulation

The main purpose of the turn insulation is to separate the turns from each other and prevent short circuits between turns. If a short circuit between turns were to occur, a similar effect as the one in an autotransformer will take place and the shorted turn will appear as the secondary side winding in an autotransformer. For example, if a winding has 100 turns and a dead short occurs across one turn then 100 times normal current will flow in the shorted turn [10, p17].

Groundwall insulation

The main purpose of the groundwall insulation is to separate and prevent short circuits between the copper conductors in the windings and the grounded stator core. In a random-wound stator the ground insulation is sometimes the same as the turn insulation meaning that the wire insulation of the turns serves as both turn and groundwall insulation. The turn insulation is designed to handle the full phase-to-phase voltage which is commonly a maximum of 600 volts. In electrical machines rated higher than 250 volts however, random-wound stators most often have sheets of insulating material along the inside of the slot walls. This of course provides additional ground insulation and make up the groundwall insulation [10, p19].

Slot divider

Many random-wound stators also have sheets of insulating material, similar to the ground wall insulation, between coils of different phases that share the same slot. This is called slot divider.

2.2 Insulation degradation

The degradation of the stator insulation is often a slow process. The stator insulation can be affected and suffer degradation from different kinds of stresses. The main stresses are electrical, mechanical, ambient and thermal stress. In general, if insulation failure is caused as a consequence of constant stress the time

until failure is proportional to the number of operating hours of the electrical machine. If the stress is of a more transient nature, such as motor starting, out-of-phase synchronisation of a generator or a lightning strike the time until failure is principally proportional to the number of transients the electrical machine experiences.[10]

2.2.1 Parasitic capacitance

Everywhere where there is electricity there is also parasitic capacitance. Parasitic capacitance or stray capacitance is a usually unwanted, unavoidable capacitance that exists between electrically conducting materials because of the proximity of the materials. The parasitic capacitance is often small and can in most cases be ignored. However the effects of the parasitic capacitance increase with frequency and at higher frequencies the parasitic capacitance at some point needs to be accounted for. [2, p199].
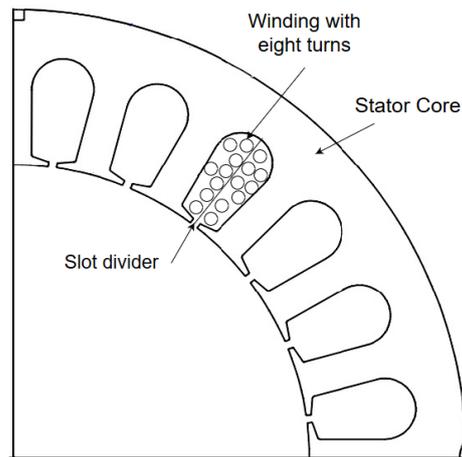
Figure 2.1: Principal drawing of the stator of a PMSM or particularly the PMSM most used during the experiments conducted during this master thesis (H5M1). This machine has 24 slots (only six drawn here). The windings are so called random wound and every winding contains eight round turns. Every slot contains two windings from different phases that are separated by a slot divider.

2.2.2 Parasitic capacitances in a PMSM

The detailed impedance structure of an electrical machine is complex. Basically there are parasitic capacitances between all conducting materials in the machine. In this thesis the parasitic capacitances are generally divided into phase-to-phase, phase-to-ground and turn-to-turn capacitance. These capacitances are mean values and should one make a complete representation and include all individual capacitances the model quickly becomes large and complicated. For instance the

turn-to-turn capacitance is not the same between all turns. It depends on a number of factors such as the distance between the turns, the position of the turns in respect to other turns, where between the turns the measurement is done etcetera. A detailed model which includes many parameters and account for many effects is presented in [1]. However for the purpose of this thesis with a strategy to keep the equivalent circuit model rather simple and because of the fact that many of the units used, such as individual turn-to-turn capacitance is difficult to measure (would require disassembling of the PMSM) an extremely detailed circuit model with many components has not been used. Instead the focus has been to use a model that contains as few parameters as possible but still account for all effects that has a large influence of how the current response from a voltage step, generated by a power converter, will behave. Representations of where the parasitic capacitances are located in a PMSM are seen in figures 2.1 and 2.2.
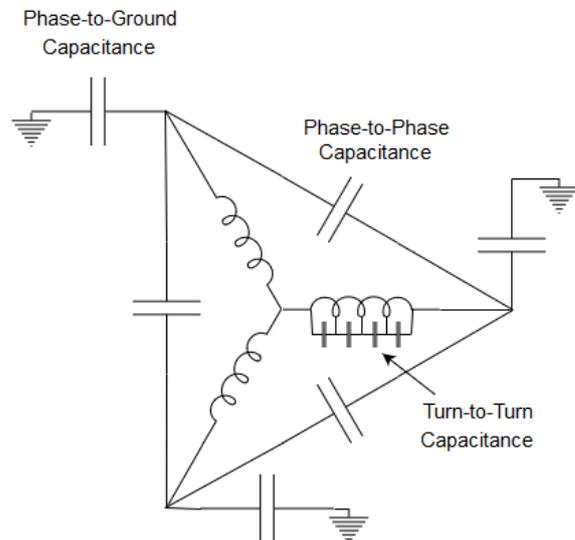
Figure 2.2: Circuit diagram representation of the parasitic capacitances in a PMSM. The electric machine is star connected and the stator windings are represented by an inductance only for simplicity. The capacitances included are the phase-to-ground capacitance; between the windings and the stator core, the phase-to-phase capacitances; amongst the windings and the turn-to-turn capacitance; between the turns of a winding.

2.2.3 Relation between insulation state and capacitance

There is a correlation between the insulation capacitance and the stator insulation quality. According to inter alia [12] the insulation capacitances decrease when the electric machine is subjected to ageing or accelerated ageing tests. How much the capacitances change when subjected to a particular ageing cycle or how much the capacitance change before a machine breakdown occurs varies between machines.

This is not that strange since different machines have different insulation thickness and materials. To know the exact relationship between these parameters, one would have to investigate the particular electrical machine in question. With this in mind, it is not unreasonable to assume that the percentage change of insulation capacitance before machine breakdown would not dramatically differ between machines. In [12], the phase-to-ground capacitance before machine breakdown had decreased by roughly 30 percent. In the same study it was also concluded that the insulation capacitance gave the most consistent result for insulation state indication when compared to insulation resistance and dissipation factor.

2.2.4 Equations

$$v(t) = L\frac{di}{dt} \tag{2.2.1}$$

Equation 2.2.1 describes the relationship between the self-inductance, L, the voltage, v(t) and the current i(t) through an electric circuit.

$$C = \epsilon_r \epsilon_0 A/d \tag{2.2.2}$$

Equation 2.2.2 describes the capacitance between two flat conducting plates. C is the capacitance in farads. ϵ_r is the relative static permittivity of the material between the conducting materials also called the dielectric constant. ϵ_0 is the electrical constant $8.854*10^{-12} F/m$. A is the area of the two conducting materials and d is the distance between the conducting materials.

2.3 Description of the Method

The method investigated in this thesis project is as previously stated an on-line method for monitoring the SoH of a PMSM. More precisely the method monitors the stator insulation system. According to different studies about a third of the machine failures of electrical machines are related to the stator [11, p131]. By only using this method one will not find all kinds of faults. Faults relating to the rotor, even though they are much less common than stator related faults, will go undetected. Faults that are related to bearings, which are the most common reason for machine failure [11, p131], are also not detected.

2.3.1 Idea

The investigated method's idea is to be simply applicable with little alteration to the hardware already used in hybrid or electric vehicles today. The idea is to use the vehicles battery and power electronics, which normally are used as energy storage and power converter to operate the vehicles electrical machine acting as motor or generator, to also diagnose the electrical machine and detect developing faults early. The measurements done would only take a fraction of a second and

could for instance be done automatically every time the key is inserted in the ignition. This thus means that the user of the vehicle would not notice or experience any inconvenience from the use of the method.

2.3.2 How it works

The method works in the following way. First a short voltage step is applied over the phases of the electrical machine in the vehicle. This voltage step can be as short as 10 μs.The voltage step is generated by the power converter going from the switch state lower short circuit (0,0,0) to, for instance, switch state (1,0,0). This corresponds to applying the DC-link voltage over the phases as depicted in figure 2.3. The transient current response that occurs as a result of this voltage step is then measured. The exact place of where the current is measured is also shown in figure 2.3.

The same measurement procedure is also done in the other phases. The only difference being that the voltage step comes from switch state lower short circuit (0,0,0) to (0,1,0) or (0,0,1) instead of (1,0,0) and that the current is measured in the corresponding phase. This makes it possible to pinpoint the insulation degradation to a specific phase or note that it is a symmetric insulation degradation in all the phases.

As previously mentioned the measurement could be done for instance every time a key is inserted into the ignition. The measurements are then stored and the changes over time can be studied. This makes it possible to see how the current response, there by the parasitic capacitances in the electrical machine and their by the stator insulation quality has changed over time. By comparing these results to a library of data stored from other similar vehicles one could see how fast the stator insulation is deteriorating and detect developing faults.

2.3.3 Need for high sampling frequency

One difficulty with this measurement is that this current transient has a high frequency. This frequency depends on the motor but the largest frequency component of the electrical machine used for measurements in experiments used in this project was about 6.7 MHz. This means that the current sensor used, for this electrical machine, has to be able to measure currents that are in the range of this frequency. It also means that the other components used such as the Analogue to Digital (AD)-converter also has to be able to handle such high frequencies. This frequency of 6.7 MHz is a lot higher than what standard current sensors used in traction machines today can measure. Upgraded or additional current sensors would thus be needed for implementation of this method.
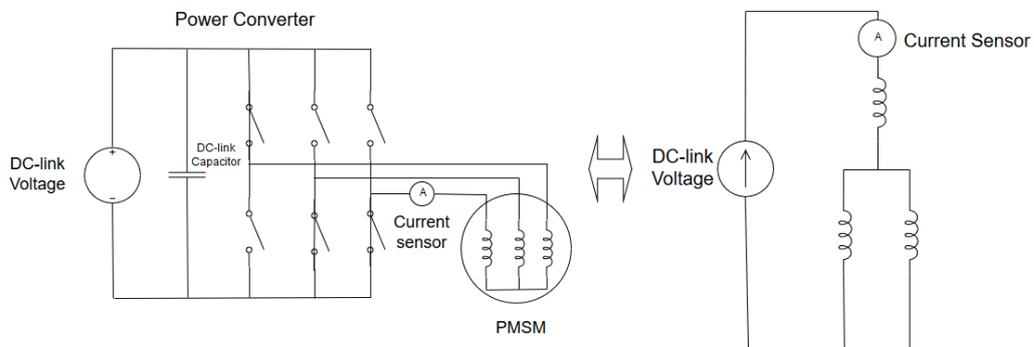
Figure 2.3: Illustration of where a voltage step is applied in the electrical machine. To the left is a representation of the status of the switches (transistors) in the power converter when a voltage step is generated. The left picture also includes how the electrical machine's windings are connected to the power converter and where the current is measured. The right circuit is equivalent with the left and shows the result of setting the switches as in the left picture.

Chapter 3

Electrical model

3.1 Construction of equivalent circuit

When constructing a circuit model for use in this project the aim was that the model should be as simple as possible but still include all significant effects that influence the behavior of the current response. The motivation and reasoning behind the electrical model's parameters is described in this chapter, starting with the calculation of the parasitic capacitances in the PMSM depicted in figure 2.2.

3.1.1 Parasitic capacitance calculation

This section contains calculations of the parasitic capacitances from phase to ground and phase to phase from the geometry of the stator of the PMSM under test.

$$C = \epsilon_r \epsilon_0 A / d \qquad (3.1.1)$$

Where:
C is the capacitance in farads
ϵ_r is the relative static permittivity of the material between the conducting materials also called the dielectric constant
ϵ_0 is the electrical constant $8.854 * 10^{-12} F/m$
A is the area of the two conducting materials ,and d is the distance between the conducting materials.

To calculate the capacitance between a phase and the iron core of the stator all the area where the two are in close contact are considered. The used dimensions and material constants are listed below.
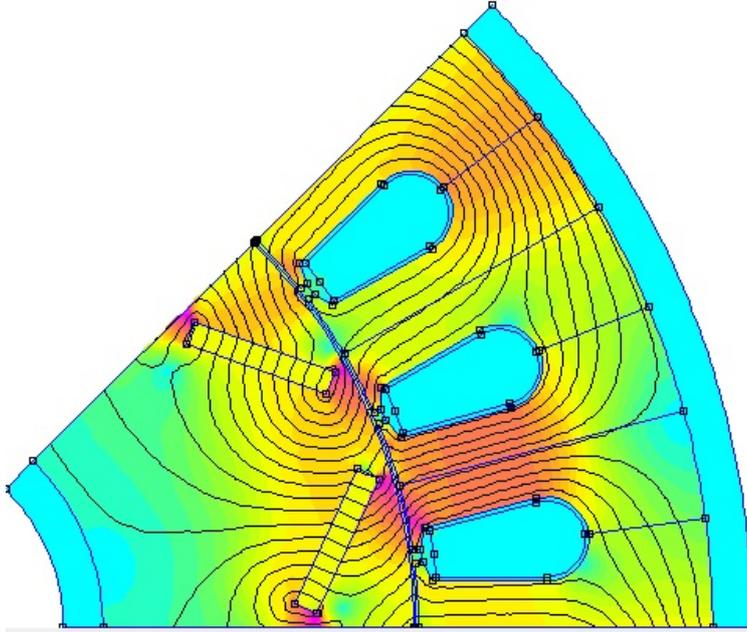
Figure 3.1: Segment of the stator from a FEM-model of the electrical machine used. Three slots are seen on this segment which is an eighth on the stator (24 slots in total). Every slot contains two coils from different phases (not seen in the picture).

- the circumference of a slot is approximately $O = 0.0525$ m.

- the number of slots in the stator is $n = 24$.

- the axial length of the slots are $L = 0.080$ m.

- the liner thickness, the distance between the winding and the slot wall, is 0.48 mm.

- Of the liner thickness, the slot insulation consisting of $d_1 = 0.31$ mm Nomex Mylar Nomex (NMN) triple layer insulation which is presumed to have a ϵ_r of 3.1. The rest of the liner thickness ($d_2 = 0.17mm$) is air which has $\epsilon_r=1$.

- The slot divider thickness $sd = 0.24$ mm. The slot divider is also made of NMN.

- Each slot contains two coils from different phases.

- Each coil contains eight turns.

- Each turn contains eight strands.

The total Area between one winding and the iron core is calculated as $A = O * L * n * \frac{1}{3} = 0.0336 \ m^2$.

The fact that it is two materials between the conducting materials makes two capacitances in parallel. The first of those with NMN insulation with a ϵ_r of 3.1 is calculated to $C_1 = \frac{3.1\epsilon_0 * A}{d_1} = 1.75$ nF.

The second of these two parallel capacitances which have air ($\epsilon_r = 1$) between the conducting materials is calculated to $C_2 = \frac{\epsilon_0 * A}{d_2} = 2.7830$ nF.

This gives the total phase to core capacitance $\frac{1}{C_{phasetocore}} = \frac{1}{C_1} + \frac{1}{C_2} -> C_{phase-to-core} = 1.0744$ nF.

The phase to phase capacitance is calculated in a similar manner. The area between the conductors in this case is calculated to $A_{ptp} = 0.01929 * n\frac{1}{3}L = 0.02469$ mm^2. The total phase to phase capacitance is then calculated to $C_{phasetophase} = \frac{\epsilon_0 * A_{ptp}}{/sd} = -> C_{phasetophase} = 1.3208$ nF

Some assumptions and simplifications are made in these calculations. One being that the coil in the used model is flat rather than consisting of eight round turns as it does in reality. This simplification influence the distance between the iron core and the coil which in reality is a bit different around the coil. For this reason, to get an idea of how much this will influence the result, the calculations has also been done with the distance of air between the conductors being 0.05 and 0.1 mm greater. This results in the following :
0.17 mm of air distance (default) gives $C_{phasetocore} = 1.074$ nF.
0.22 mm of air distance gives $C_{phasetocore} = 0.910$ nF.
0.27 mm of air distance gives $C_{phasetocore} = 0.789$ nF.
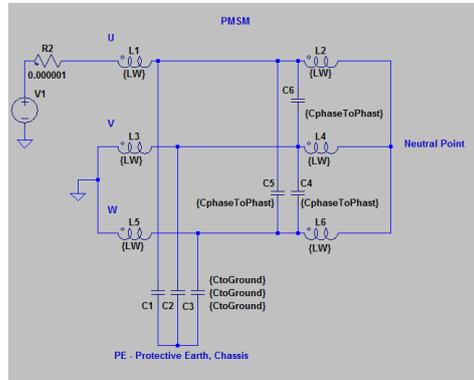
Figure 3.2: Equivalent circuit model of the electrical machine under test. Not seen in this picture is the mutual inductive coupling factor between the phase windings. Also not seen in the picture are the series resistance of the winding inductances.

3.1.2 Description of the model

The electrical simulation model can be seen in figure 3.2. The model includes the three phases of the electrical machine in star configuration. The power converter

is represented by a voltage source that is set to produce a voltage step with the same properties as the voltage step in reality in terms of magnitude, rise time and pulse width. Every phase winding is represented by two inductances in series. The main reason for this compared to only having every phase represented by one inductance is that the parasitic capacitances in the model now can be connected in the middle of the winding instead of at the beginning or in the end of a winding. This influences the behavior of the circuit. The inductances also have a series resistance. The values used for the inductances and series resistances are taken from measurements done with an impedance analyser. The measurements with the impedance analyser are attached to this report and can be seen in (Apendix A).

The phase-to-ground parasitic capacitance is connected between the mid points of each winding to a common node in the model representing the chassis. The phase-to-phase parasitic capacitances are connected directly between the mid points of the phase windings, equivalent with a delta connection. Both the phase-to-ground and phase-to-phase capacitances used in the model have both been measured with an impedance analyser and calculated from the known geometry of the stator. The measurements with the impedance analyser are attached to this report and can be seen in (Apendix A). The calculations of the capacitances can be seen earlier in this chapter under the section Parasitic capacitance calculation.

3.1.3   Mutual Inductance

The developed electrical model also accounts for the mutual inductance between the phases of the electrical machine. The mutual inductance is represented by a magnetic coupling factor between all of the phases. The coupling factor between the two inductances that belongs to the same phase is presumed to be high, $k = 0.99$. The coupling factor between the first phase and the other two are set to -0.5. This comes from the assumption that all windings magnetomotive force are ideally sinusoidally distributed. This makes the phase windings shifted 120 electrical degrease from each other which corresponds to a coupling factor of $k = Cos(120°) = -0.5$. The coupling factor between the two last phases in the model is $k = cos(-120°) = cos(240°) = -0.5$.
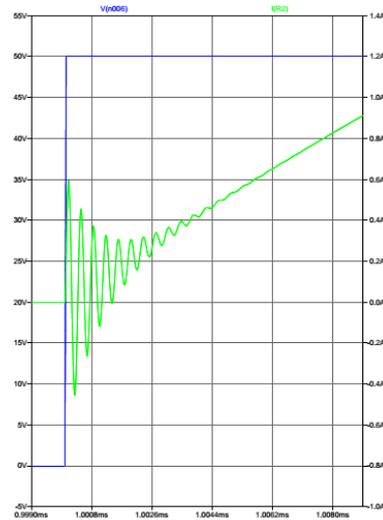
Figure 3.3: Current response from the simulation model without any simulated fault. The green curve is the current and the blue one is the voltage.

3.2   Simulated current response

The final developed circuit is seen in 3.2. A simulated current response from a 50 volt voltage step is seen in figure 3.3. The step is chosen to be 50 volts in the simulation model and in the measurements. The same voltage level for all carried out test was kept at 50 volts to have consistency and to be able to compare results between measurements as easy as possible. The exact amount of 50 volt is chosen because the capacitors used for the simulated faults are rated to 50 volts. The voltage level is in no way limited to be this low and could just as easily have been chosen to another value.

Chapter 4

Experimental Procedure

4.1 Implementation

The experiments conducted during this master thesis project were done in the M-building at Faculty of Engineering - Lund University (LTH) in Lund in the elaboration room named Lab 6. The tests have mainly been performed on a PMSM referred to as H5M1 Hägglunds BAE. If nothing else is mentioned then that means that this electric machine was used. Some additional tests has also been carried on a similar, but not exactly alike, machine referred to as H5M2 IEA LTH and some tests has been done on a different, larger PMSM referred to as Rasmus' machine. The purpose of these additional test has been mainly to try the method on other machines and compare the results. The equipment used is found in list-form under the header Equipment used 4.1.7.

4.1.1 Test Set-up

The test set-up consists of the PMSM itself, motor control as well as high frequency current sensing and logging. A block diagram of the set-up is seen i figure 4.1. The PMSM is placed on an a large iron foundation which is grounded (Protective Earth). The electric machine is star connected through a connection box to the power converter which is located inside an electrical cabinet. The cables used are shielded except for a short distance of approximately one decimetre before and after the connection box. The cable length between the PMSM and the power converter is proximately three meters. The cable is of the type ölflex classic 110 cy 4 g 16 rohs, 1135624. The power converter that runs the PMSM is controlled with a Compact Reconfigurable Input Output (cRIO). The current sensor used is placed around one of the phase cables between the power converter and the PMSM. When measurements are conducted in another phase the current sensor is moved to that particular phase cable. The current logging is done on a Red Pitaya

which for the intents and purposes of this thesis basically is a fast AD-converter, a Field-Programmable Gate Array (FPGA) and a memory.
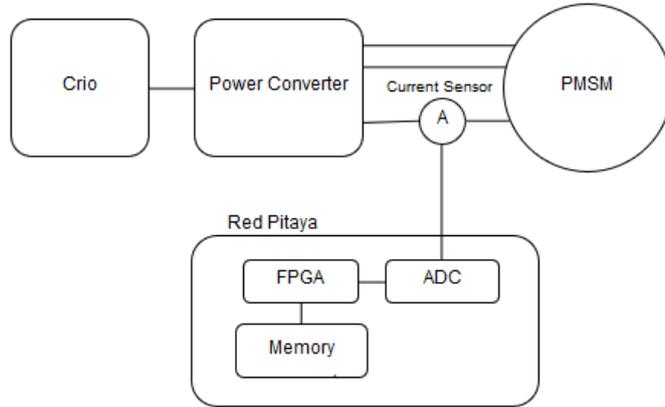
Figure 4.1: Block diagram of the test set-up.

4.1.2 Test object 1

As stated in the introduction to this section the main test object is called H5M1 Hägglunds BAE. A picture of this machine can be seen in figure 4.2. It is a six pole, three phase PMSM with the power ratings 12 kW continuous and 22 kW peak power. It has a maximum speed rated to 15000 revolutions per minute (rpm) and a peak torque of 100 Nm. Furthermore the stator contains 24 slots with two windings per slot. Each winding consists of eight turns which in turn consists of eight strands of copper. [6].

4.1.3 Test object 2

For some additional test a larger eight pole, 18 slots PMSM has been used. A picture of this machine can be seen in 5.15. This machine is rated to 80 kW continuous and 180 kW peak power. It has a peak torque of 250 Nm and a maximum speed of 15000 rpm. The machine is a prototype build and designed by Rasmus Andersson and is referred to as Rasmus' machine. This machine has been used to carry out tests to evaluate temperature dependency since this machine is equipped with five Pt-100 temperature sensors. It has also been used in the purpose of trying out the method on a larger machine and a machine with six instead of eight poles.[3]

4.1.4 Motor Control

The PMSM is run by a 3-phase power converter controlled by a cRIO system. A specific program for control of the PMSM for the purpose of this fault detection

Figure 4.2: Picture of the PMSM under test.

method has been developed and programmed in Labview. Both the cRIO system and the Labview software are products of National Instruments. The developed control program is written so that voltage pulses of variable pulse width can be generated corresponding to going from switch state (0,0,0,) to (1,0,0,), (0,1,0,) and (0,0,1,) respectively. The pulse width can be varied from one tenth of a micro second and up. The limit of this tenth of a micro second is a consequence of how the program is written and the internal clock of the cRIO FPGA. The program uses four ticks of the internal FPGA clock for one loop and one tick takes 25 nano seconds. The dc-link voltage, that for these active switch states also becomes the voltages over the windings, can be manually regulated through a variable transformer. The dc-link voltage can be varied at least between 15 and 400 volts.

4.1.5 Current measurement

The phase current is measured with the current probe A6303 and the current probe amplifier Tektronix AM 503 when the machine is subjected to a voltage step. This current sensor is able to measure currents up to 60 MHz. The current sensor is connected to a Red Pitaya which is a circuit board containing among other things an FPGA , a processor and Random Access Memory (RAM) . The Red Pitaya also has fast Analogue to Digital Converters (ADCs) and their by fast analogue inputs. The Red Pitaya's analogue inputs has a sample rate of 125 Mega Samples per second (MS\s). It was also tried to measure the current response with a CWT Rogowski current probe named CWT3B but it proved to have to low resolution to accurately display the current response.

4.1.6 Data logging

The Red Pitaya which is programmed in MATLAB is programmed in such a way that it triggers on a rising voltage slope on one channel and measure the high frequency current on a second channel. The program is written so that when the data buffer is filled with data, which takes 131 micro seconds, the program is automatically directly ready to trigger on a new voltage pulse and take new measurements. This makes it very easy to quickly do, for instance, a series of ten measurements just by applying ten fast voltage pulses with the motor control program written in Labview. For the purpose of verifying the function of the Red Pitaya measurements was done were data gathered by the Red Pitaya was compared with the data obtained from an oscilloscope.

4.1.7 Equipment used

Most of the equipment used is described more thoroughly in other sections. Here is the most relevant equipment used in list form.

- Red Pitaya

- Current probe A6303 and the current probe amplifier Tektronix AM 503

- cRIO system

- Cable of the type Ölflex classic 110 cy 4 g 16 rohs, 1135624.

4.1.8 Performed tests

A large number of tests are performed. All of the test results that are used comes from a mean value of ten different current responses from ten different measurements done with the same settings. Firstly the current response is measured separately in each of the three phases; U,V and W. Then, the current response is also measured in all the three phases separately for four different rotor positions. These measurements only becomes $10 * 3 * 4 = 120$ measurements. Measurements with different dc-link voltage of 50 and 100 volts are also made. In order to simulate a fault or a developing fault measurements are done with different capacitors placed in parallel with one phase. Measurements are then performed and analysed for both the phase parallel with the fault and the other phases. To study the influence of the cables used measurements with the current probe placed as close to the inverter as possible, instead of right before the electrical machine, are also done. Measurements with an electrical machine in higher temperature are also done to study if a warmer machine effects the results of the measurements.

4.2 Data Analysis

The data analysis is done in MATLAB. A program is written that stores the data collected by the Red Pitaya on a computer. The data is analysed in the time and frequency domain. The MATLAB-program does some post processing of the data and is able to produce a comparative fault indicator value that is based on the difference in frequency content from healthy measurements and the recently taken measurements. The MATLAB program is also able to plot the current response in the time and frequency domain. More details of what post processing the data goes through is found in the chapter 5 Analysis and results .

Chapter 5

Analysis and results

5.1 Characteristics of the current response

A plot of a standard current response from a voltage step is seen in figure 5.1. The current response has some characteristic properties. First, at the instance of the voltage step there are high frequency oscillations. After some micro seconds these oscillations ring out and the curve converts to an increasing curve with a constant derivative. This increase with constant derivative is consistent with an inductive circuit, see 2.2.1.
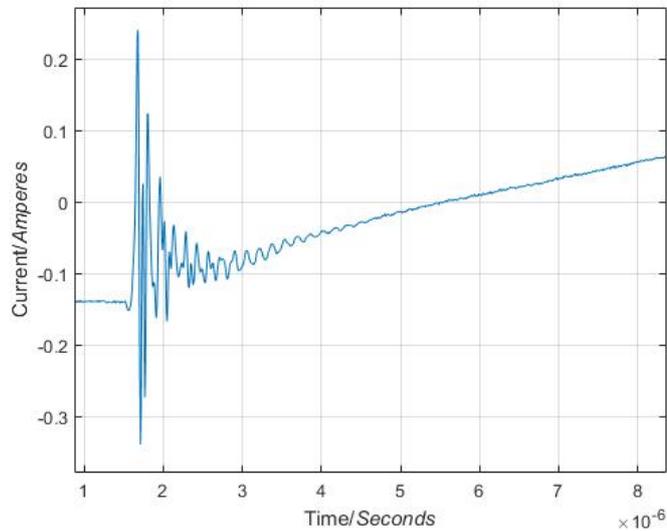
Figure 5.1: Current responses from a 50 V voltage step with a pulse width of 10 μs. The current is measured in phase U. The graph is constructed from mean values of ten measurements. Notice the high frequency oscillations in the beginning of the response that later rings out and the graph turns into a curve increasing with a constant derivative.

5.2   Repeatability and comparison with oscilloscope

The measurements are repetitive in the sense that the results from measurements done with the same settings and conditions deviate from each other very little. This is illustrated in figures 5.2 and 5.3 which shows ten different measurements plotted in the same graph. Figure 5.3 is the same as 5.2 but more zoomed in. Measurements were the results obtained from the Red Pitaya were compared with the ones obtained from an oscilloscope was also done. A plot with both results from an oscilloscope and the Red Pitaya can be seen if figure 5.4. It can be seen that the difference between the two is extremely small.
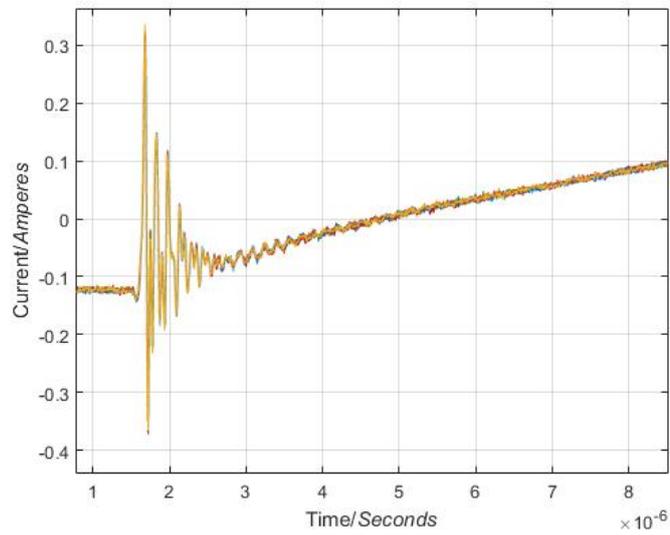
Figure 5.2: Plot with 10 measurements of current responses from 50 V voltage steps with a pulse width of 10 μs.
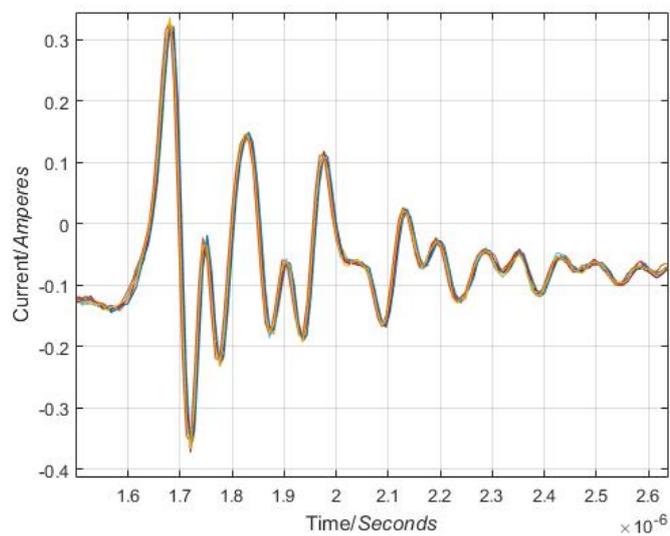
Figure 5.3: Plot with 10 measurements of Current responses from 50 V voltage steps with a pulse width of 10 μs. Same as 5.2 but more zoomed in.
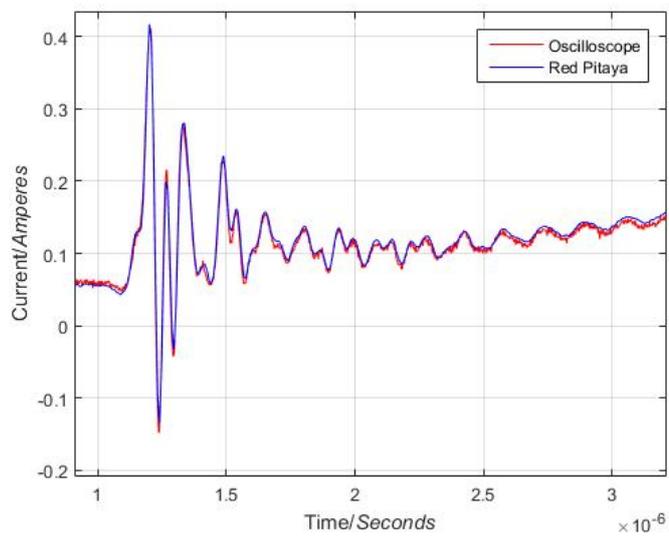
Figure 5.4: Plot with measurements from both the Red Pitaya and an oscilloscope.

5.3   Rotor position dependency

The inductance of the PMSM depends among other things on rotor position, see 5.5 and Appendix A. It would however be practical for this method to be independent of the rotor position. Otherwise the rotor position would have to be the same for all measurements which would require some solution for placing the rotor in a specific position or at least determine the rotor position. This might not be that difficult but it would in any case be preferable to not need to do it. Hence, it would be beneficial to exclude this inductive part of the curve from the plot. This is done simply by subtracting the constant current derivative from the curve. More precisely it is done by fitting the right part of the curve to the closest first degree polynomial and then this polynomial is subtracted from the curve.
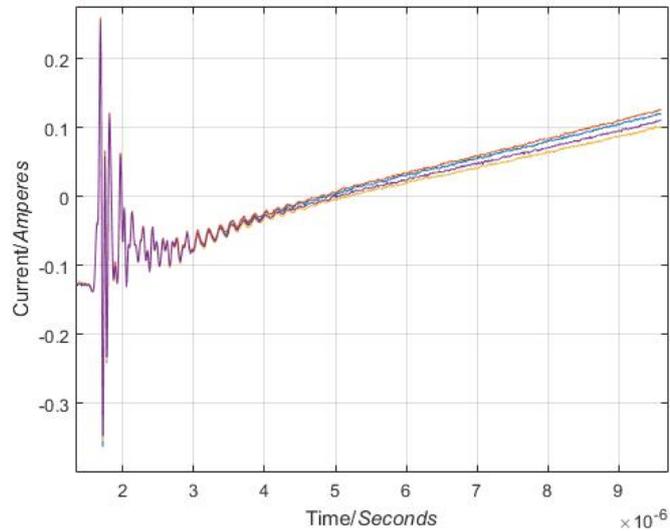
Figure 5.5: Current responses from measurements with four different rotor positions. Notice the difference mainly seen to the right in the plot.
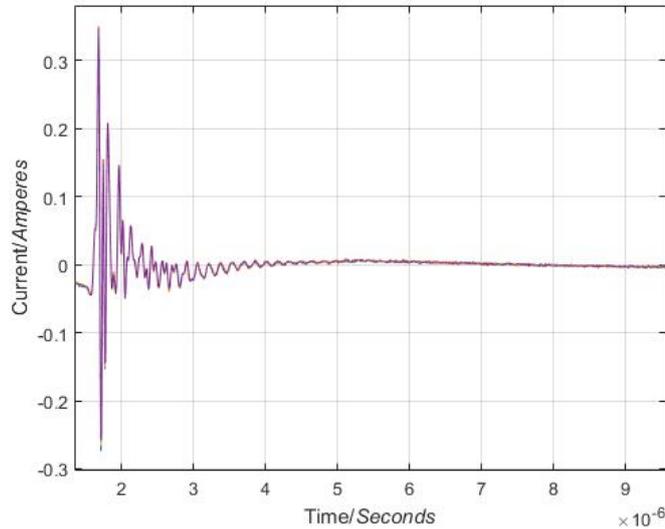
Figure 5.6: Current responses from measurements with four different rotor positions after the subtraction of the constant current derivative. Notice that the earlier difference between the for curves, seen in figure 5.5,now is difficult to observe at all.

5.4   Effects of changed parasitic capacitance

The current response can be studied either in the time or frequency domain. Both these approaches are pursued. In figures 5.8 and 5.9 the effects of a simulated fault of 1 nF parallel with one phase can be observed in the time and frequency domain respectively. An illustration of where the fault capacitor is placed is seen in figure 5.7. In both plots, but perhaps most easily in 5.9, it can be seen that the main frequency is lower when a 1 nF capacitor is connected in parallel with one phase. This is expected since a capacitor in parallel corresponds to an increase in capacitance which leads to a decrease in resonance frequency. One way to notice a change of the parasitic capacitances could thus be to look at what frequency the highest peak in the amplitude spectrum is through Fast Fourier Transform (FFT). Another way is look at the difference in amplitude spectrum at a certain frequency band.
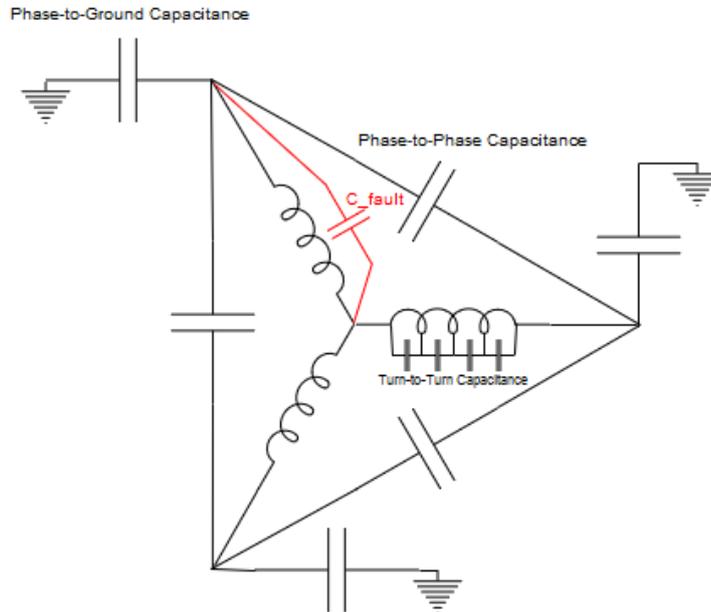
Figure 5.7: Illustration of where the fault capacitor, the simulated fault, is added in the circuit. It is placed parallel to phase U.
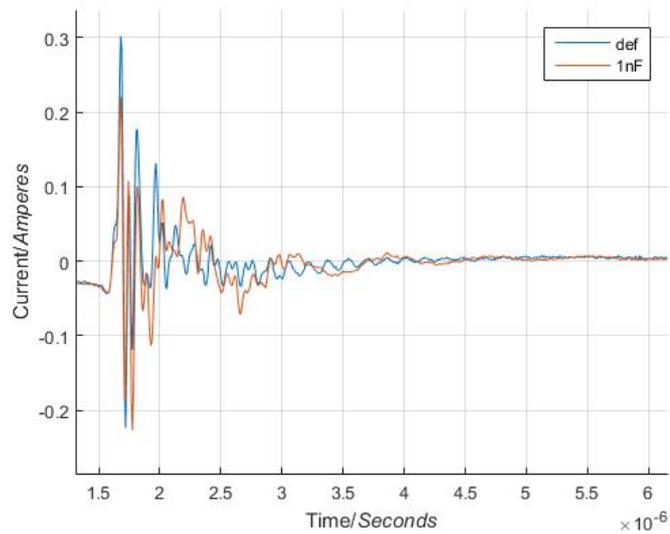
Figure 5.8: Current responses from measurements with a simulated fault. The voltage step used is of 50 V. The blue curve is from the default set-up and the red curve is from measurements done with a 1 nF capacitor in parallel with phase U.

5.5   Difference in frequency content

In figure 5.8 there is a clear difference in frequency content in the current response
when a fault of 1 nF is present. But what is a good way to identify a fault or a
developing fault through use of the amplitude spectrum and how small faults can
be detected and distinguished from noise. This is investigated. In figure 5.10 the
difference between the FFT:s of current responses can be seen.
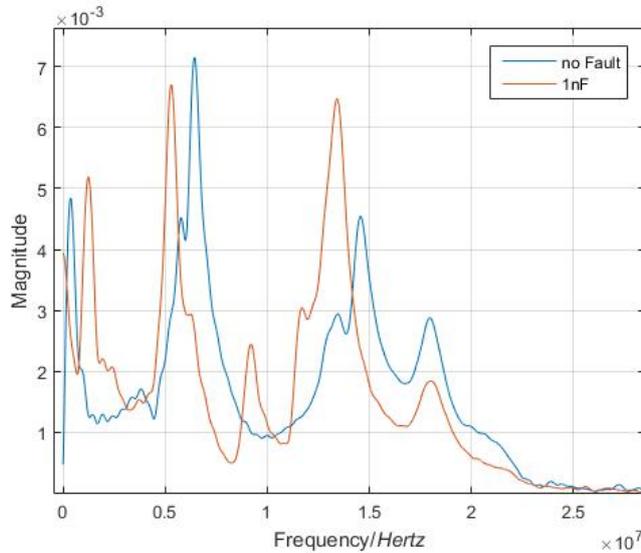
Figure 5.9: Amplitude spectrum of the current responses from a 50 V voltage step
of 10 us applied in phase U. The blue curve is from the default set-up without any
fault capacitor and the red curve is from measurements done with a 1 nF capacitor
in parallel with one phase as showed in figure 5.7

5.6   Accuracy

An important and interesting factor for a method such as the one proposed in this
thesis is to know how small of a change that can be detected using the method.
More precisely for this method this means to be able to say with certainty that the
observed change is from a change of the impedance of the PMSM and not from
any noise, disturbance or any other error source. In order to do this measure-
ments with simulated faults of different capacitances are analysed and a way to
produce a numeric comparative fault indicating value is developed. A plot of the
difference in amplitude spectrum from measurements with different fault capaci-
tors can be seen in figure 5.10. Figure 5.11 illustrates how much a measurement
can deviate from the original curve without necessarily being a sign of a developing
fault. The figure shows the absolute value of the difference in amplitude spectrum

from measurements with different fault capacitors. It also includes the difference in amplitude spectrum between different measurements of a healthy machine at different rotor positions.
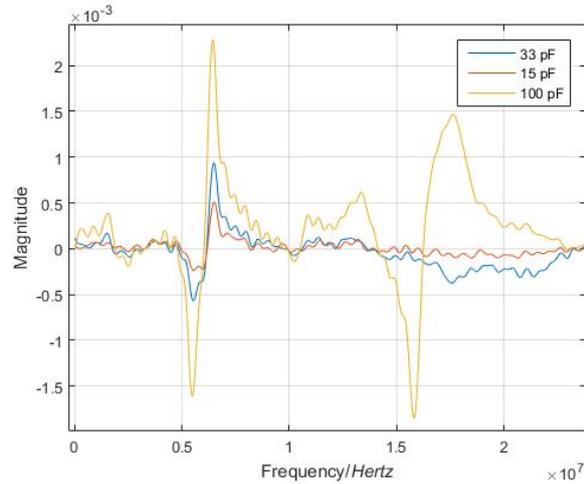
Figure 5.10: Difference in amplitude spectrum between measurements with a fault capacitors added in parallel to one phase and measurements from a healthy machine. Essentially the default amplitude spectrum with no fault capacitor subtracted with the amplitude spectrum of the current response with a fault capacitor connected in parallel.

Figure 5.11: Absolute value of the difference in amplitude spectrum from measurements with different fault capacitors. Three graphs from similar measurements from a healthy machine at different rotor positions are also included. The healthy machine measurements are the red curves.

Fault condition	Fault Indicator Value
100 pF	7.54
33 pF	2.59
15 pF	1.02
Error threshold value	0.94

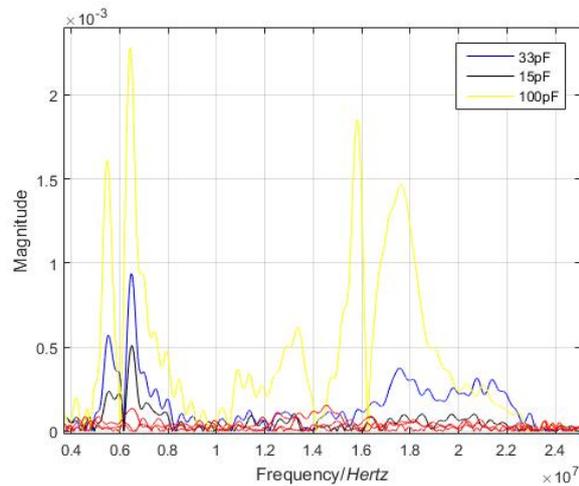Table 5.1: Shows the single phase fault indicator value for some different simulated faults. The error threshold value, the value that the fault indicator value needs to be higher than to statistically ensure that a change of impedance has occurred, is also included.

5.7   Comparative fault indicator value

A way to produce a comparative numeric value which indicates the severity of a developing fault is suggested here. The proposed method is based on comparing the difference in the amplitude spectrum of a recent series of measurements with corresponding measurements from a healthy machine. The way to reach this fault indicator value goes as follows. First the amplitude spectrum where the most frequency content is present is chosen. For the studied machine in this project it was chosen to be between 3.75 and 25 MHz. This can be seen for instance in figure 5.10. Then the absolute value of the difference at every frequency (steps of 1250 Hz) is summed up. This becomes 1700 values. This sum then becomes the Fault Indicator Value.

This fault indicator value can be constructed from measurements from the three different phases. By doing so it is possible to see in what phase the developing fault is located or if it is a symmetrical fault. Values from measurements in the three phases with a fault capacitor of 100 pF parallel with phase U, can be seen in 5.2.

5.7.1   Error threshold value

The meaning of, and the way the error threshold value is reached is covered here. In short it is a value that the fault indicator value needs to be higher than to statistically ensure that a change of impedance has occurred. This value is reached in the following way. Twelve series of measurements were every series of measurements consists of the mean value from ten measurements were taken. These twelve series of measurement were from the three different phases with four different rotor positions. Then the steps for generating the fault indicator value were taken for all the combinations of rotor positions for each phase. Meaning comparing rotor position one through four in all six combinations possible for the three phases. This gives 18 values. The mean value, standard deviation and 95 percent confidence interval were then calculated. The mean value was 0.5633 and the standard deviation was 0.1534. If normal distribution is presumed then the 95 percent confidence interval from these parameters with 18 measurements is +-0.07, meaning that the mean value of the whole distribution, with a 95 percent probability, is

Fault condition	Measured phase	Fault Indicator Value
100 pF parallel phase U	U	8.22
100 pF parallel phase U	V	2.06
100 pF parallel phase U	W	2.24

Table 5.2: Shows the Fault Indicator Value from measurements from the three different phases from a simulated fault of 100 pF parallel to phase U.

within the interval 0.5633+-0.07. Then if normal distribution again is presumed the fault indicator value has to be over $0.5633 + 0.07 + 2*0.1534 = 0.9401$ to with a 95 percent certainty guarantee that a change of impedance has occurred. This value is called the error threshold value. The factor two in the calculation comes from that two standard deviations corresponds to the 95.4 percent percentile in normal distribution.

5.8   Influence of current sensor location

To study if and how much the measurements would be affected if the current probe was placed closer to the power converter, measurements with the current probe placed as close to the power converter as possible were done. This means that the current probe was placed at the same cable but roughly three meters closer to the converter. The results of the series of measurements done showed that the the current response indeed was significantly different. The two different current responses can be seen in figure 5.12 and the amplitude spectrum of the signals can be seen in figure 5.13. The biggest reason for this large difference in high frequency current is probably the parasitic capacitance of the cable itself. Even though the capacitance between the different conductors and between the conductors and ground is small it still has a rather great influence at the high frequencies (approximately 7 MHz) that are studied. An equivalent circuit representation of a cable can be seen in figure 6.1. This makes the accuracy of the, in this thesis, suggested fault detection technique susceptible to moving of the current sensors or changing of the cables between the power converter an the electric machine.
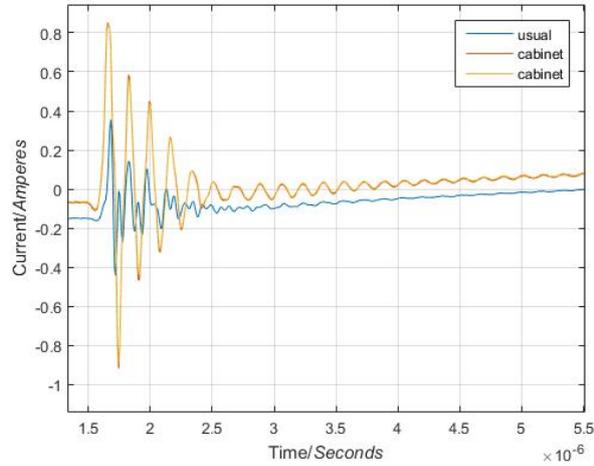
Figure 5.12: High frequency current response right before the electric machine (usual) and right after the power converter (cabinet). The word cabinet refers to that the current probe was placed inside the cabinet containing the power converter etcetera. In the plot there are measurements from two series of measurements from the cabinet.
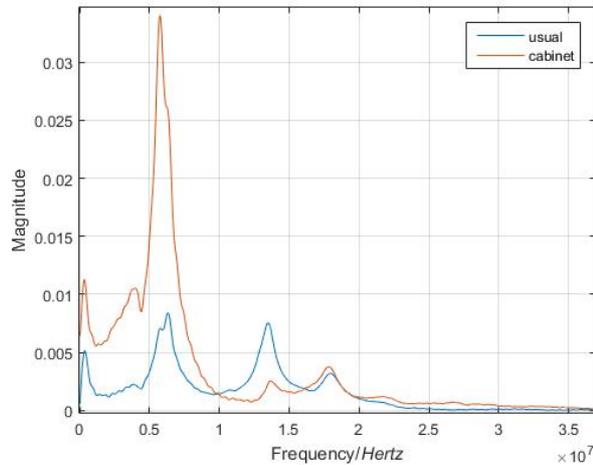

Figure 5.13: Amplitude spectrum of the current response right before the electric machine (usual) and right after the power converter (cabinet).

5.9   Thermal dependency

To analyse the thermal dependency a series of measurements have been done with a PMSM placed inside an isolated cage. These test was not done on the PMSM

Sensor number	Sensor name	Description
1	$U_{hotspot}$	Located at the expected hot spot, halfway along the machine in the middle of a slot in one of the phases (phase U)
2	$U_{statorback}$	Located at the stator back outside the slot containing sensor 1
3	NDE	Located at the bearing on the non-driving end
4	DE	Located at the bearing on the driving end
5	$U_{endwinding}$	Located on the end windings from the slot containing sensor 1 (phase U)

Table 5.3: The temperature sensors of the PMSM under thermal test.

most used in this project but on another, larger PMSM, referred to as Rasmus' machine. Measurements have first been done in room temperature, about 23 degrees and then with the machine at a temperature of approximately 50 degrees. The machine was heated externally with a heating gun. The measurements were done when the temperature sensors had stabilised after the heating process. The electrical machine used for these measurements has five PT100 RTD temperature sensors. A table of where these are placed is seen in table 5.3 and a picture of the placement is seen in figure 5.14. A table of the status of the sensors before and after heating is shown in table 5.4. Pictures of the machine under test and the thermal cadge used is shown in figures 5.15 and 5.16.
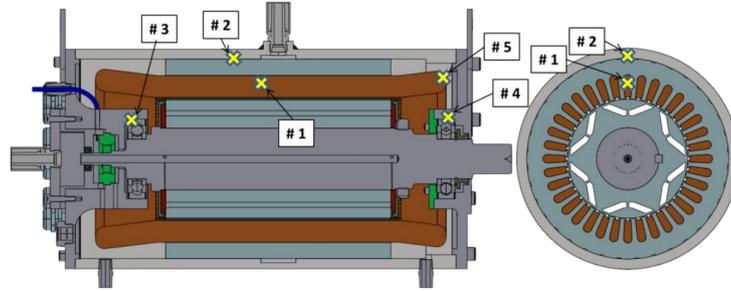
Figure 5.14: Temperature sensor positions in the PMSM used for thermal tests.

It might be difficult to see from the amplitude spectrum in figure 5.17 but it is easily seen in the zoomed-in version in figure 5.18 that there is a small change in frequency content when the machine is 50 degrees Celsius compared to when it is 23 degrees. The earlier described fault indicator value for the heated machine from these measurements becomes approximately 1.5 which means that it is higher than the error threshold value of 0.94 and thereby it is statistically certified at a 95 percent confidence rate that a change of impedance has occurred. However even though there is a change, the change is very small.

Sensor	Sensor name	R_{before}	R_{after}	T_{before}	T_{after}
1	$U_{hotspot}$	109,281	119,303	23°C	48°C
2	$U_{statorback}$	109,222	119,293	23°C	48°C
3	NDE	109,279	119,246	23°C	48°C
4	DE	109,269	119,612	24°C	49°C
5	$U_{endwinding}$	not available (n\a)	n\a	n\a	n\a

Table 5.4: Status of the temperature sensors during test. R_{before} is the resistance of the PT100 resistors before heating, at the temperature of the reference measurements. R_{after} is the resistance after heating, at the temperature of the measurements done in higher temperature. T_{before} and T_{after} are the temperatures corresponding to the resistance of the PT100 sensors.

Figure 5.15: The PMSM placed inside an isolated cage for the purpose of investigating thermal dependency.

Figure 5.16: The isolated cage containing the PMSM.
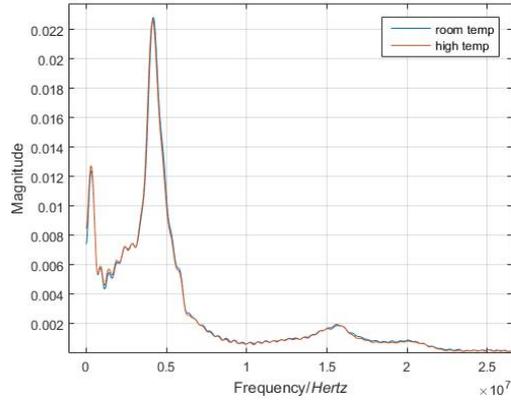
Figure 5.17: Amplitude spectrum from measurements in room temperature and at approximately 50 degrees Celsius.
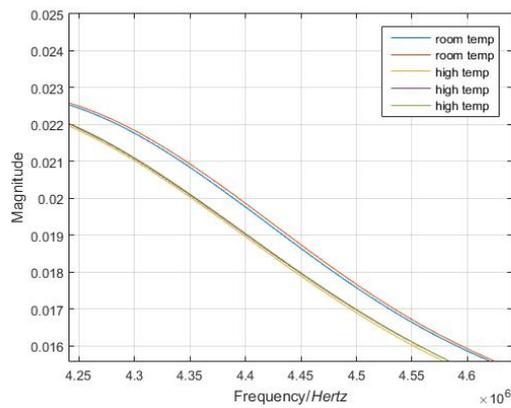
Figure 5.18: Amplitude spectrum from measurements in room temperature and at approximately 50 degrees Celsius, zoomed in.

5.9.1 Larger machine

The results from the tests done on Rasmus' machine can also be compared with the test done on the smaller machine. Compare for instance figures 5.17 with 5.9. It can be seen that the amplitude spectrum of the larger Rasmus' machine contains lower frequencies compared to the usual machine. The largest frequency content in the smaller machine's amplitude spectrum is found around the frequency 6.7 MHz compared to 4.5 MHz for Rasmus' machine. This means that the current sensor and the data logging equipment needed can be slightly slower for Rasmus' machine.

Chapter 6

Comparison of model and measurements

If the measurements done are compared to the results given from the simulation model some difference can be noted. If the comparison is done between figures 5.1 and 3.3 which are current responses from a 50 volt voltage step from measurements contra the simulation, the behavior, amplitude and frequency of the oscillations are quite similar to the results obtained from the measurements. However, one directly notices that the simulation gives a much cleaner and more regular current response compared to the measured one. The simulated signal has a clear dominating frequency which basically make up the whole signal compared to the measured signal that consists of more spread frequencies. In figure 5.12 a plot from measurements where the current probe were placed right after the power converter, before the cable, can be seen. One notice that the current response from this measurement is more similar to the plot obtained from the simulation (figure 3.3). This could be because the simulation does not account for the cable. Right after the power converter the current looks more like the simulation but after the cable the high frequency current transient looks a bit different. At the high frequency, that the current transient has, the parasitic elements of the cable seems to have quite a large effect. Therefore a simulation model with a model of the cable also included was constructed.
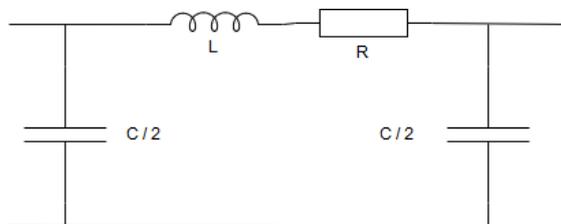
Figure 6.1: Circuit representation of a cable.
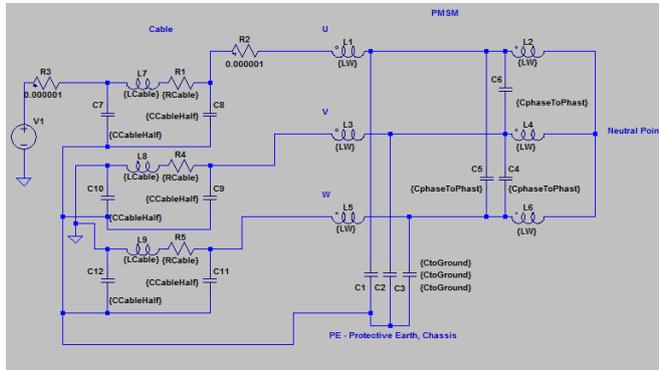
Figure 6.2:   Equivalent circuit model of the electrical machine under test with a model of the cables connecting the PMSM to the power converter also included. The current is measured right before phase U, after the cable.
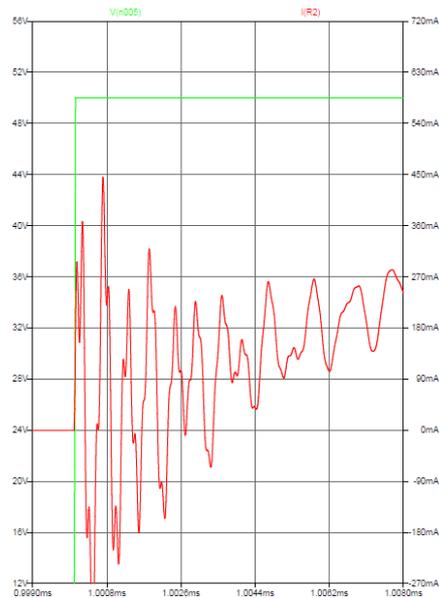
Figure 6.3:   Current response from the simulation model with a cable model added as in figure 6.1. The red curve is the current and the green one is the voltage.

It is noticeable that the new simulated current response is more similar to the measured values obtained in the sense that the frequency content is more spread. The behavior in terms of frequency and amplitude is in the same range as the measurements. However the similarities stops there. To simulate a current response that in detail looks like the measured current response a better model is needed.

Chapter 7

Conclusion and future work

7.1 Conclusion

This method for detecting developing faults in the stator insulation looks promising. It is shown that small changes of insulation (corresponding to a 15 pF capacitor parallel with a phase) can be detected with the method and equipment used in this thesis project. This small of an impedance change is estimated to occur long before a stator insulation fault is present. In this sense the method works satisfactory. There is no reason for this method not to work that has been found during this master thesis project. There are however some aspects that the implementer of this method needs to be aware of. These are listed below.

- First of all the method does not detect all kinds of faults but only faults relating to the stator insulation. It does not detect rotor or bearing related faults. However a method that detects 37 % of all failures, which is the approximate number of how many failures that are related to stator winding problems according to [10][p131], before they occur, is still highly interesting.

- It is difficult to, with precision, relate how much the current response can change before a fault occurs. To do this one would need data from other similar machines that has been run until breakdown. One can however make a less exact estimation based on simulated faults.

- The proposed method is highly sensible to movement of the current sensor to another place on a cable or changing anything that influences the impedance structure of the circuit consisting of the power converter, the electrical machine and the cables between them. Knowing this one could however work around this issue.

- The method requires that current of a high frequency can be measured and

logged.

7.1.1   Hardware requirements

One of this thesis project purposes was to look into what the minimum hardware requirements would be to implement this method in a vehicle. This basically comes down to one thing. The current needs to be measured and logged at a high frequency which require a fast current sensor as well as a fast ADC. Other than this the equipment needed for implementation is basically already present in a hybrid or electric vehicle today. Exactly how high of a frequency that needs to be measured varies between machines. For the machine most tested in this thesis project, currents at at least five MHz needs to be able to be measured. This is illustrated for example in figure 5.11 where it can be seen that the frequency content difference between a healthy machine and one with a simulated fault is significantly smaller below circa 5 MHz. This means that the sampling needs to be significantly faster than this and thereby the current sensor and the ADC needs to be significantly faster than 5 MHz.

7.2   Suggestions for Future work

7.2.1   More extensive testing

To fully evaluate this method a good approach would be to do the measurements on some healthy, identical, electrical machines and then subject the machines to enhanced ageing while taking measurements along the way. This would have to be done until machine breakdown occurs for the machines. This would generate a library of data that could be compared with other machines. Then hopefully it could be determined with high precision and likelihood how long a particular machine is from insulation break down.

7.2.2   Better electrical model

With more knowledge and time it would be possible to improve the electrical model. With a more sophisticated model it might be possible to , amongst other things, analyse certain small changes in the current response and be able to see which type of impedance change in the electrical machine a particular change of the current response corresponds to.

References

[1]   Fadi Abdallah. "EMC Analysis of Electric Drives". Licentiate Thesis. Lund University, 2012.

[2]   Kenneth W. Alley Charles L.; Atwood. *Electronic Engineering, 3rd Ed.* New York John Wiley & Sons., 1973. ISBN: 0-471-02450-3.

[3]   Rasmus Andersson. "Electric Traction Machine Design for Heavy Hybrid Vehicles". Licentiate Thesis. Lund University, 2014.

[4]   S. Grubic, J. Restrepo, J. M. Aller, Bin Lu, and T. G. Habetler. "A New Concept for Online Surge Testing for the Detection of Winding Insulation Deterioration in Low-Voltage Induction Machines". In: *IEEE Transactions on Industry Applications* 47.5 (Sept. 2011), pp. 2051–2058. ISSN: 0093-9994. DOI: 10.1109/TIA.2011.2161972.

[5]   G. M. Joksimovic and J. Penman. "The detection of inter-turn short circuits in the stator windings of operating motors". In: *IEEE Transactions on Industrial Electronics* 47.5 (Oct. 2000), pp. 1078–1084. ISSN: 0278-0046. DOI: 10.1109/41.873216.

[6]   F. J. Márquez-Fernández, Z. Huang, and M. Alaküla. "Redesign of an Electrical Rear Wheel Drive (E-RWD) for a hybrid vehicle in a given drive cycle". In: *Electrical Machines (ICEM), 2012 XXth International Conference on.* Sept. 2012, pp. 2702–2708. DOI: 10.1109/ICElMach.2012.6350268.

[7]   P. Nussbaumer, T.M. Wolbank, and M.A. Vogelsberger. "Separation of disturbing influences on induction machine's high-frequency behavior to ensure accurate insulation condition monitoring". In: *Applied Power Electronics Conference and Exposition (APEC), 2013 Twenty-Eighth Annual IEEE.* Mar. 2013, pp. 1158–1163. DOI: 10.1109/APEC.2013.6520445.

[8]   José Rodríguez. Senior Member. IEEE. Luis Morán. Senior Member. IEEE. Jorge Pontt. Member. IEEE. Ruben Osorio and Samir Kouro. "Modeling and analysis of common-mode voltages generated in medium voltage PWM-CSI drives". In: *Power Electronics, IEEE Transactions on* 18.3 (May 2003), pp. 873–879. ISSN: 0885-8993. DOI: 10.1109/TPEL.2003.810855.

[9] F. Perisse, P. Werynski, and D. Roger. "A New Method for AC Machine Turn Insulation Diagnostic Based on High Frequency Resonances". In: *Dielectrics and Electrical Insulation, IEEE Transactions on* 14.5 (Oct. 2007), pp. 1308–1315. ISSN: 1070-9878. DOI: 10.1109/TDEI.2007.4339494.

[10] G. C. Stone, E. A. Boulter, I. Culbert, and H. Dhirani. *Electrical insulation for rotating machines-design, evaluation, aging, testing, and repair.* the Institute of Electrical and Electronics Engineer Inc., 2004.

[11] G. C. Stone, E. A. Boulter, I. Culbert, and H. Dhirani. *Electrical insulation for rotating machines-design, evaluation, aging, testing, and repair.* the Institute of Electrical and Electronics Engineer Inc., 2004, p. 131.

[12] S. J. Williamson, R. Wrobel, J. D. Booker, J. Yon, and P. H. Mellor. "Effects of Insulation Ageing on the Conductive Heat Transfer from the Winding Body into Machine Periphery/Stator Core Pack". In: - - (2016).

[13] J. Yang, J. Cho, S. B. Lee, J. Y. Yoo, and H. D. Kim. "An Advanced Stator Winding Insulation Quality Assessment Technique for Inverter-Fed Machines". In: *IEEE Transactions on Industry Applications* 44.2 (Mar. 2008), pp. 555–564. ISSN: 0093-9994. DOI: 10.1109/TIA.2008.916753.

[14] C. Zoeller, M.A. Vogelsberger, R. Fasching, W. Grubelnik, and T.M. Wolbank. "Evaluation and current-response based identification of insulation degradation for high utilized electrical machines in railway application". In: *Diagnostics for Electrical Machines, Power Electronics and Drives (SDEMPED), 2015 IEEE 10th International Symposium on.* Sept. 2015, pp. 266–272. DOI: 10.1109/DEMPED.2015.7303700.

Appendix

Winding and insulation impedances

Test object H5 (Gröna Bilen Redesign, Termoos prototypes: M1 Hägglunds BAE and M2 IEA LTH)

HM8118 is used to series RL across the winding terminals and parallel RC between terminals and machine housing
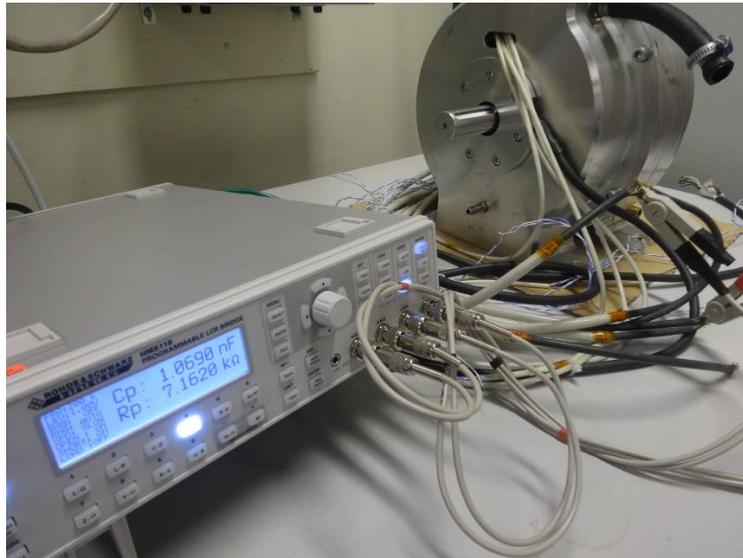
Measurement	Description	Test sample
H5M1_UU_P1	RL-ser Pos:1 Ph:U-m V-o W-o	200Hz 1.26mH 114mΩ 2kHz 1.23mH 1022mΩ
H5M1_VV_P1	RL-ser Pos:1 Ph:U-o V-m W-o	200Hz 1.12mH 113mΩ 2kHz 1.10mH 949mΩ
H5M1_WW_P1	RL-ser Pos:1 Ph:U-o V-o W-m	200Hz 1.85mH 130mΩ 2kHz 1.80mH 1213mΩ
H5M1_UC_P1	RC-par Pos:1 Ph:UC-m V-o W-o	200Hz 1.33nF 13.0MΩ 2kHz 1.30nF 4.54MΩ
H5M1_VC_P1	RC-par Pos:1 Ph:U-o VC-m W-o	200Hz 1.35nF 11.7MΩ 2kHz 1.32nF 4.31MΩ
H5M1_WC_P1	RC-par Pos:1 Ph:U-o V-o WC-m	200Hz 1.33nF 13.1MΩ 2kHz 1.30nF 4.53MΩ
H5M1_UV_P1	RC-par Pos:1 Ph:U-m V-m W-o	200Hz 1.02nF 16.7MΩ 2kHz 0.99nF 6.27MΩ
H5M1_UW_P1	RC-par Pos:1 Ph:U-m V-o W-m	200Hz 1.03nF 16.6MΩ 2kHz 1.01nF 6.27MΩ
H5M1_VW_P1	RC-par Pos:1 Ph:U-o V-m W-m	200Hz 1.03nF 16.6MΩ 2kHz 1.01nF 6.27MΩ
H5M1_UU_P2	RL-ser Pos:2 Ph:U-m V-o W-o	200Hz 1.98mH 130mΩ 2kHz 1.91mH 1495mΩ
H5M1_VV_P2	RL-ser Pos:2 Ph:U-o V-m W-o	200Hz 1.12mH 114mΩ 2kHz 1.09mH 978mΩ
H5M1_WW_P2	RL-ser Pos:2 Ph:U-o V-o W-m	200Hz 1.27mH 122mΩ 2kHz 1.25mH 1040mΩ
H5M1_UC_P2	RC-par Pos:2 Ph:UC-m V-o W-o	200Hz 1.33nF 12.9MΩ 2kHz 1.30nF 4.54MΩ
H5M1_VC_P2	RC-par Pos:2 Ph:U-o VC-m W-o	200Hz 1.34nF 11.7MΩ 2kHz 1.31nF 4.31MΩ
H5M1_WC_P2	RC-par Pos:2 Ph:U-o V-o WC-m	200Hz 1.33nF 13.2MΩ 2kHz 1.30nF 4.52MΩ
H5M1_UV_P2	RC-par Pos:2 Ph:U-m V-m W-o	200Hz 1.01nF 16.6MΩ 2kHz 0.99nF 6.29MΩ
H5M1_UW_P2	RC-par Pos:2 Ph:U-m V-o W-m	200Hz 1.01nF 17.6MΩ 2kHz 0.99nF 6.42MΩ
H5M1_VW_P2	RC-par Pos:2 Ph:U-o V-m W-m	200Hz 1.03nF 16.5MΩ 2kHz 1.01nF 6.26MΩ
H5M1_UU_P3	RL-ser Pos:3 Ph:U-m V-o W-o	200Hz 1.17mH 114mΩ 2kHz 1.14mH 1023mΩ
H5M1_VV_P3	RL-ser Pos:3 Ph:U-o V-m W-o	200Hz 1.92mH 127mΩ 2kHz 1.87mH 1367mΩ
H5M1_WW_P3	RL-ser Pos:3 Ph:U-o V-o W-m	200Hz 1.23mH 121mΩ 2kHz 1.21mH 997mΩ
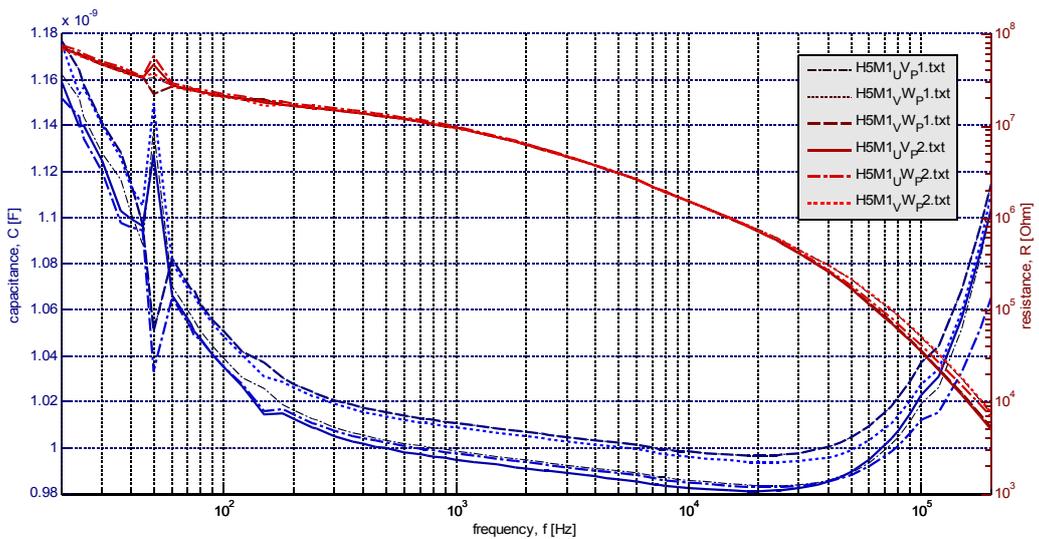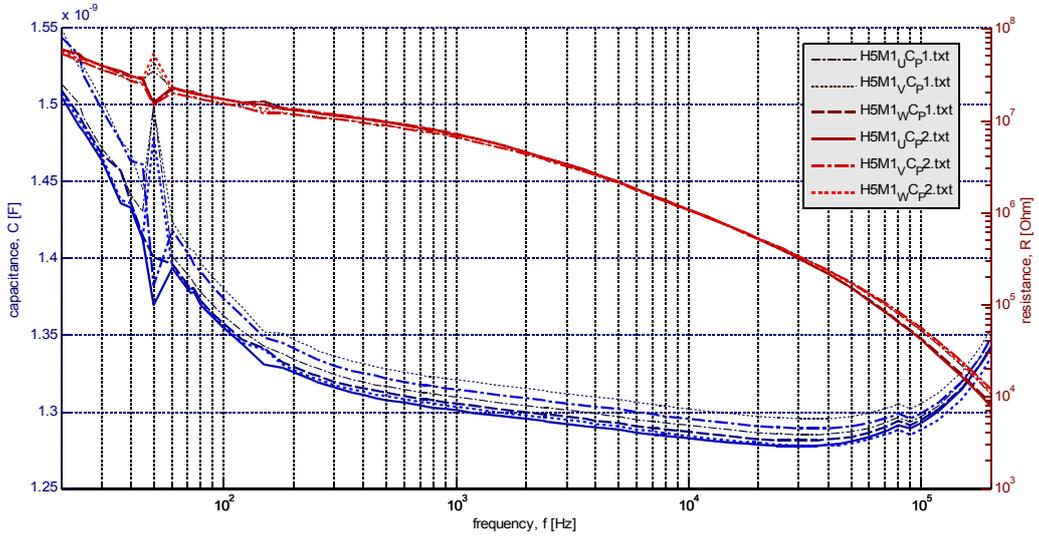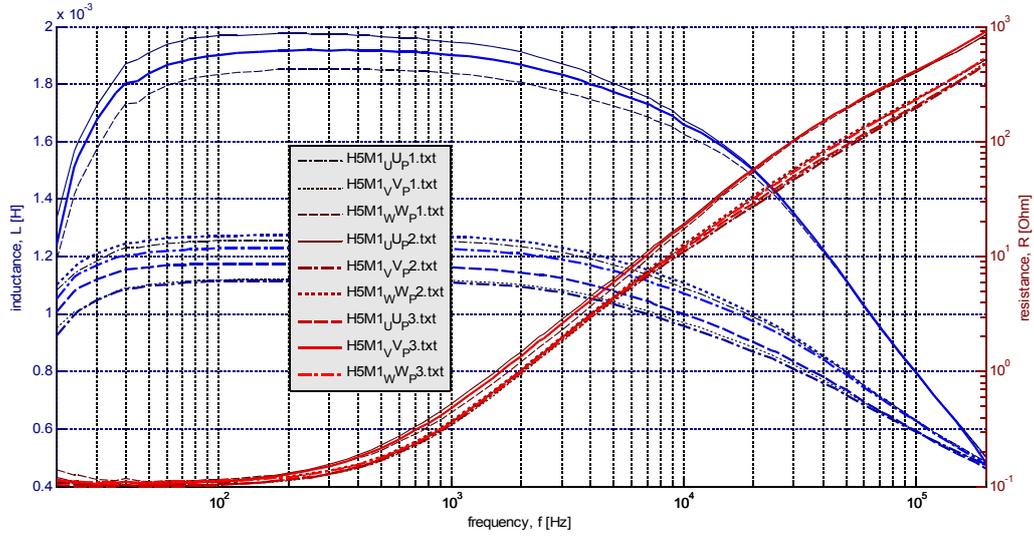
Measurement	Description	Test sample
H5M2_UU_P1	RL-ser Pos:1 Ph:U-m V-o W-o	200Hz 1.17mH 44mΩ 2kHz 1.15mH 788mΩ
H5M2_VV_P1	RL-ser Pos:1 Ph:U-o V-m W-o	200Hz 1.07mH 40mΩ 2kHz 1.06mH 767mΩ
H5M2_WW_P1	RL-ser Pos:1 Ph:U-o V-o W-m	200Hz 1.74mH 47mΩ 2kHz 1.69mH 876mΩ
H5M2_UC_P1	RC-par Pos:1 Ph:UC-m V-o W-o	200Hz 1.33nF 13.0MΩ 2kHz 1.30nF 4.54MΩ
H5M2_VC_P1	RC-par Pos:1 Ph:U-o VC-m W-o	200Hz 1.35nF 11.7MΩ 2kHz 1.32nF 4.31MΩ
H5M2_WC_P1	RC-par Pos:1 Ph:U-o V-o WC-m	200Hz 1.33nF 13.1MΩ 2kHz 1.30nF 4.53MΩ
H5M2_UV_P1	RC-par Pos:1 Ph:U-m V-m W-o	200Hz 1.02nF 16.7MΩ 2kHz 0.99nF 6.27MΩ
H5M2_UW_P1	RC-par Pos:1 Ph:U-m V-o W-m	200Hz 1.03nF 16.6MΩ 2kHz 1.01nF 6.27MΩ
H5M2_VW_P1	RC-par Pos:1 Ph:U-o V-m W-m	200Hz 1.03nF 16.6MΩ 2kHz 1.01nF 6.27MΩ
H5M2_UU_P2	RL-ser Pos:2 Ph:U-m V-o W-o	200Hz 1.89mH 58mΩ 2kHz 1.84mH 1240mΩ
H5M2_VV_P2	RL-ser Pos:2 Ph:U-o V-m W-o	200Hz 1.14mH 42mΩ 2kHz 1.12mH 871mΩ
H5M2_WW_P2	RL-ser Pos:2 Ph:U-o V-o W-m	200Hz 1.22mH 42mΩ 2kHz 1.20mH 893mΩ
H5M2_UC_P2	RC-par Pos:2 Ph:UC-m V-o W-o	200Hz 1.33nF 12.9MΩ 2kHz 1.30nF 4.54MΩ
H5M2_VC_P2	RC-par Pos:2 Ph:U-o VC-m W-o	200Hz 1.34nF 11.7MΩ 2kHz 1.31nF 4.31MΩ
H5M2_WC_P2	RC-par Pos:2 Ph:U-o V-o WC-m	200Hz 1.33nF 13.2MΩ 2kHz 1.30nF 4.52MΩ
H5M2_UV_P2	RC-par Pos:2 Ph:U-m V-m W-o	200Hz 1.01nF 16.6MΩ 2kHz 0.99nF 6.29MΩ
H5M2_UW_P2	RC-par Pos:2 Ph:U-m V-o W-m	200Hz 1.01nF 17.6MΩ 2kHz 0.99nF 6.42MΩ
H5M2_VW_P2	RC-par Pos:2 Ph:U-o V-m W-m	200Hz 1.03nF 16.5MΩ 2kHz 1.01nF 6.26MΩ
H5M2_UU_P3	RL-ser Pos:3 Ph:U-m V-o W-o	200Hz 1.20mH 46mΩ 2kHz 1.18mH 931mΩ
H5M2_VV_P3	RL-ser Pos:3 Ph:U-o V-m W-o	200Hz 1.95mH 55mΩ 2kHz 1.89mH 1250mΩ
H5M2_WW_P3	RL-ser Pos:3 Ph:U-o V-o W-m	200Hz 1.24mH 45mΩ 2kHz 1.21mH 990mΩ